

Article

Study on the Characteristics and Mechanism of Shield Tunnel Mud Cake Disintegration in Complex Red-Bed Geology

Jinshuo Yan, Xingwei Xue, Chaofan Gong and Kexin Zhang *

School of Transportation and Geomatics Engineering, Shenyang Jianzhu University, Shenyang 110168, China; 13994235269@163.com (J.Y.); gdansys@163.com (X.X.); 18203699196@163.com (C.G.)

* Correspondence: jt_zkx@sjzu.edu.cn

Abstract: The complex red-bed geology is primarily composed of iron-rich sedimentary rock layers with clay minerals as a major component. The soil water content exceeds 30%, and its high viscosity and water content lead to the easy formation of mud cake on the cutterhead, endangering the safety and progress of construction, which poses a significant challenge for tunnel boring machines (TBMs). The use of dispersants to eliminate mud cake is a common method in engineering projects. This paper presents an improved disintegration experiment instrument to study the disintegration characteristics of mud cake from the red-bed geology under different dispersant solutions, proposing a dispersant formulation suitable for the red-bed geology of the Haizhu Bay Tunnel project. The results indicate that mud cake samples exhibit a moderate disintegration effect in pure water. Furthermore, it has been observed that the disintegration effect decreases as the thickness of mud cake increases. Sodium silicate solution was not suitable for treating the red-bed geological mud cake, while sodium hexametaphosphate and oxalic acid solutions had a good promoting effect on the disintegration of red-bed geological mud cake. However, there was a threshold for the dispersant concentration; exceeding this threshold actually worsened the disintegration effect. Ultimately, the engineering application of a 10% oxalic acid solution, which proved effective in disintegrating the mud cake, significantly enhanced the excavation efficiency in the Haizhu Bay Tunnel project.

Keywords: TBM; cutterhead mud cake; complex red-bed geology; disintegration experiment; dispersant solution; engineering application



Citation: Yan, J.; Xue, X.; Gong, C.; Zhang, K. Study on the Characteristics and Mechanism of Shield Tunnel Mud Cake Disintegration in Complex Red-Bed Geology. *Coatings* **2024**, *14*, 567. <https://doi.org/10.3390/coatings14050567>

Academic Editor: Valeria Vignali

Received: 9 April 2024

Revised: 29 April 2024

Accepted: 30 April 2024

Published: 2 May 2024



Copyright: © 2024 by the authors. Licensee MDPI, Basel, Switzerland. This article is an open access article distributed under the terms and conditions of the Creative Commons Attribution (CC BY) license (<https://creativecommons.org/licenses/by/4.0/>).

1. Introduction

As urbanization accelerates, the demand for underground transportation and infrastructure construction has steadily increased. The shield tunneling method, known for its efficiency and safety, has been extensively applied in urban underground projects. However, challenges such as complex geological and hydrological conditions, the insufficient understanding of sediment improvement mechanisms, and inappropriate sediment improvement techniques can lead to frequent occurrences of mud cake formation during excavation in high-viscosity soil layers [1–4]. Mud cake refers to semi-solid or solid blocks formed by the reaggregation of clay particles and fragments cut by the cutterhead. The formation of mud cake can slow down the advancement of the shield machine, increase torque and thrust, cause wear on the tools, and potentially lead to serious accidents like surface subsidence or heaving [5–12].

Traditional methods for mud cake removal involve manually entering pressurized or atmospheric chambers to remove the mud using high-pressure water cutting or mechanical means [13]. Alternatively, injecting dispersants through the existing foam lines of the shield machine into the cutterhead and excavation chamber offers a safer and quicker solution [14]. Numerous scholars have investigated dispersants. Zhao et al. [15] validated through experiments that dispersants reduce the adhesive strength of clay, thereby mitigating the risk of mud cake formation. Langmaack et al. [16–18] analyzed the adaptability

of various improvement agents in different strata through case studies and laboratory tests, highlighting that dispersants can reduce the risk of excavation head blockage and enhance tunneling efficiency. Wang et al. [19] evaluated the impact of different types and concentrations of dispersants on the adhesion between clay and metal surfaces through a series of laboratory tests and simulation experiments. Anagnostou et al. [20] investigated the effects of dispersants on the adhesiveness of excavated clay and equipment blockage in fluid-supported excavations. The primary dispersants used to condition the slurry were poly (acrylic acid, sodium salt), poly (acrylamide-co-acrylic acid), methyl cellulose, and sodium carboxymethyl cellulose (CMC). Oliveira et al. [21] assessed the impact of different improvement agents on soil adhesion using an improved “Hobart” mixer which is produced by Hobart Corporation in USA. Thewes et al. [22,23] and Zumsteg et al. [24] advocated for the modification of spoil by adding foam and dispersants to prevent cutterhead mud caking, focusing primarily on the mechanism of action of foam agents and dispersants. Feinendegen et al. [25,26] and Spagnoli et al. [27] explored the impact of chemical solutions on clay adhesion, suggesting that certain electrolyte solutions could weaken the adhesion effect of clay. Ren et al. [28] examined the influence and mechanism of flocculants on dispersant effectiveness, proposing suitable ratios for silty clay. Sun et al. [29] conducted indoor simulation experiments on mud modification (mixing tests, slump tests, slide tests, anti-adhesion tests) and compared the improvement effects on cobblestone, pebble, and sand layers, proposing mud modification ratios suitable for engineering projects.

The engineering background of this research is the Haizhu Bay Tunnel in Guangzhou, which spans Haizhu District and Panyu District. The tunnel originates on the north side of Nanzhou Road and extends southward beneath the Zhujiang Lijiao Waterway, Luoxi Island, and the Sanzhixiang Waterway, terminating at Nanpu Avenue (Figure 1). With a total length of 2077 m, the tunnel comprises two separated tunnels running east and west, each with a diameter of 14.5 m. This engineering project is characterized by high water content, high viscosity, high rock strength, and complex mineral composition, which is not only the largest diameter shield river-crossing tunnel in Guangzhou but also ranks among the most challenging shield tunnels to construct in China due to its complex geological conditions and construction difficulties.



Figure 1. Geographical location of Haizhu Bay Tunnel.

The tunnel geology primarily features red-bed geology, mainly consisting of red conglomerate, hematite, bauxite, calcareous cement, silty clay, and muddy siltstone varying from completely to slightly weathered. Muddy siltstone, as depicted in Figure 2, is a signif-

icant geological component with a silt content of about 25% to 50% and a clay content of 50% to 75%, making clay the dominant material. Consequently, these geological conditions significantly increase the risk of mud cake formation during shield tunneling operations.

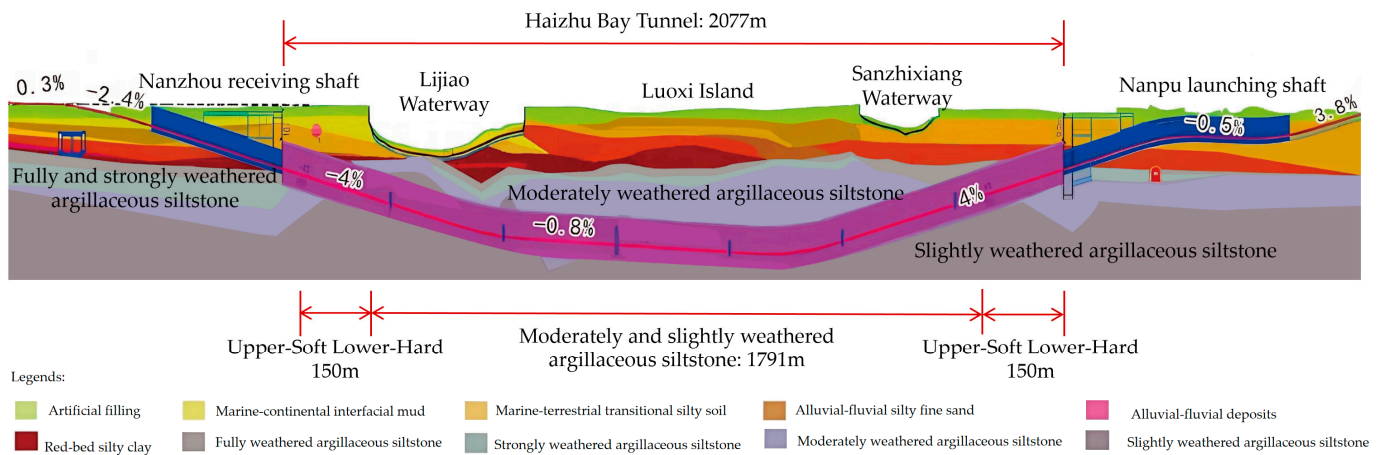


Figure 2. Longitudinal geological section.

For the east and west lines, the tunnel employs super-large-diameter slurry-balanced shield machines. In the west, there’s a pressurized cutterhead with an opening rate of about 35%, while the east uses a normal pressure cutterhead with an opening rate of about 30%. Both shield machines have a cutterhead diameter of 15.07 m (Figure 3), and their relatively small opening rates can hinder the flow of excavated soil and mud. This can easily result in the formation of mud cake on the face of the cutter heads.



Figure 3. Cutterhead of west and east lines. (a) Cutterhead of west line; (b) cutterhead of east line.

In this study, the disintegration experiment instrument was improved, and different dispersants and their optimal decomposition concentration were studied, aiming to provide theoretical foundations and engineering application references for addressing mud cake issues in red-bed geology.

2. Materials and Methods

2.1. Materials

2.1.1. Sample of Mud Cake

The excavation of the west line up to the 73rd ring encountered complex geological conditions, primarily composed of muddy siltstone intermixed with fine sand and calcare-

ous nodules. These conditions led to an increase in the shield machine's thrust and torque, a decrease in speed and penetration rate, and significant fluctuations in excavation parameters. Consequently, a decision was made to manually remove the mud cake by opening the chamber. The extracted mud cake was then sealed in plastic wrap and transported to the laboratory for analysis, as depicted in Figure 4a.

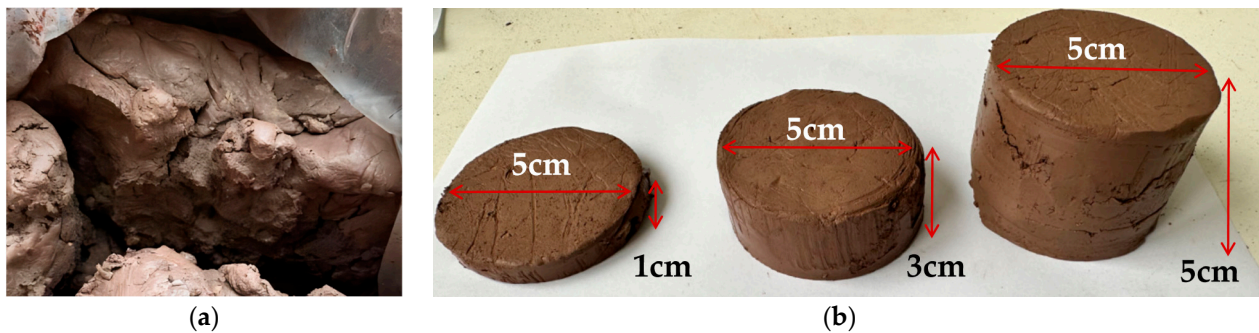


Figure 4. Mud cake. (a) Undisturbed mud cake soil sample; (b) mud cake test samples.

The basic physical properties of the measured mud cake samples are shown in Table 1, with a moisture content of 15.13%.

Table 1. Basic physical properties of the mud cake.

Moisture Content (%)	Natural Moisture Content (%)	Density (g/cm ³)	Dry Density (g/cm ³)
15.13	36.5	2.06	1.79

The mineral composition of the mud cake was obtained through X-ray diffraction (XRD) testing (Table 2). It was mainly composed of silt, clay minerals and micritic calcite, with a particle size of less than 0.0075 mm, accounting for about 68% of the total content of mud cake.

Table 2. Mineral composition of the mud cake.

Silt Clastic	Silt Particle	Clay Mineral	Limonite	Sericite	Microcrystalline Calcite
25%	20%	35%	6%	1%	13%

In the experiment, mud cake samples with diameters of 5 cm and thicknesses of 1 cm, 3 cm, and 5 cm were obtained using a ring cutter for disintegration testing (Figure 4b).

2.1.2. Dispersants

As illustrated in Figure 5, the experiment used common dispersants typically found in engineering, all of which were obtained from Wuxi Yatai United Chemical Co., Ltd. The main characteristics of the dispersants are as follows: (a) sodium silicate, containing 19.3 to 22.8% Na₂O, is a grayish-white powder that dissolves in water to form an alkaline solution; (b) oxalic acid, with a purity of 99.5% C₂H₂O₄, is a colorless crystal that becomes acidic when dissolved in water; and (c) sodium hexametaphosphate, containing 65 to 70% P₂O₅, is a white powder that becomes alkaline upon dissolving in water. Additionally, pure water was used in the experiment for comparison as water is also a commonly used dispersant.



Figure 5. Dispersants. (a) Sodium silicate; (b) oxalic acid; (c) sodium hexametaphosphate.

2.2. Specimens

By studying the disintegration of mud cake with thicknesses of 1 cm, 3 cm, and 5 cm in pure water, the disintegration pattern and characteristic of mud cake disintegration under pure water conditions and identified suitable mud cake thicknesses for subsequent experiments could be obtained. A total of 3 samples were examined, named PW-T1, PW-T3, and PW-T5, where “PW” represents pure water, “T” and the following numbers represent the thickness, and the specific thickness values and the specific thickness values are given in centimeters.

Solutions of sodium silicate, sodium hexametaphosphate, and oxalic acid, mixed with pure water in defined ratios, were prepared to have mass percentages of 2%, 4%, 6%, and 8% for both sodium silicate and sodium hexametaphosphate, along with 5%, 10%, and 15% for oxalic acid solutions. These solutions were utilized to assess the disintegration impact of varying dispersant concentrations on mud cake in red-bed geology. In Table 3, “SS”, “SH”, and “OA” stand for sodium silicate, sodium hexametaphosphate, and oxalic acid, respectively. The “P” followed by numbers indicates the mass percentage of each solution.

Table 3. The specimens for the experiment.

Specimens	Percentage of Dispersant (%)	Thickness of Mud Cake (cm)	Initial Moisture Content of Mud Cake (%)	Explanation
PW-T1	/	1	15.13%	Pure water
PW-T3	/	3	15.13%	
PW-T5	/	5	15.13%	
SS-P2	2%	3	15.13%	Sodium silicate solutions with different concentrations
SS-P4	4%	3	15.13%	
SS-P6	6%	3	15.13%	
SS-P8	8%	3	15.13%	
OA-T3-P5	5%	3	15.13%	Oxalic acid solutions with different concentrations
OA-T3-P10	10%	3	15.13%	
OA-T3-P15	15%	3	15.13%	
SH-T3-P2	2%	3	15.13%	Sodium hexametaphosphate solutions with different concentrations
SH-T3-P4	4%	3	15.13%	
SH-T3-P6	6%	3	15.13%	
SH-T3-P8	8%	3	15.13%	

2.3. Experimental Methods

In this study, the Gouy–Chapman–Stern double-layer model was applied to explore the disintegration mechanism of the mud cake (as discussed in Section 2.3.1). An improved disintegration experiment instrument (as detailed in Section 2.3.2) was used to conduct

disintegration tests on mud cakes with various dispersants to determine the optimal type and concentration of dispersants (as described in Section 3). The technical roadmap for this research is shown in Figure 6.

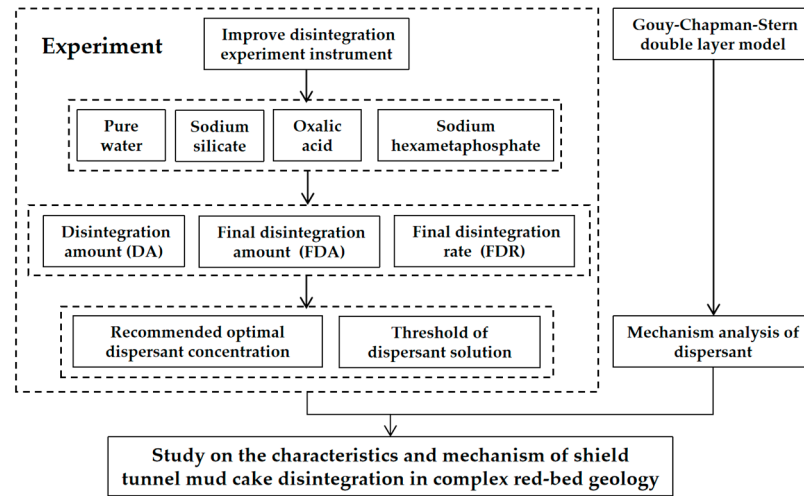


Figure 6. Technical roadmap.

2.3.1. Disintegration Mechanism

Soil particles in the mud cake, placed in a dispersant solution, undergo ionic dissociation between the surface minerals of the particles and the dispersant. This process forms a layer of negatively charged soil particles (NCSPs) on the surface of the particles, as illustrated in Figure 7. To maintain overall electrical neutrality, NCSPs adsorb cations from the dispersant solution, creating a compact Stern layer around the soil particles. Additionally, a charge-balanced transition solution region exists between the Stern layer and the dispersant solution, known as the diffusion layer [30–33].

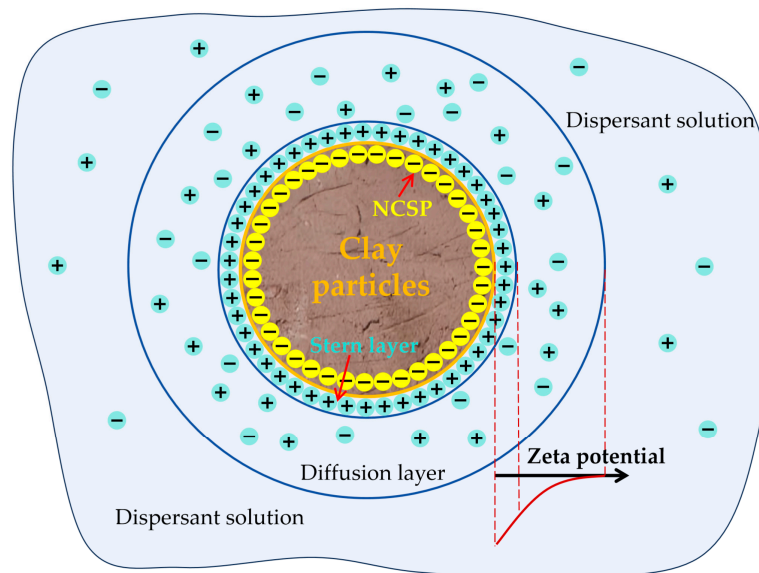


Figure 7. Gouy–Chapman–Stern double-layer model.

The Stern layer and the diffusion layer jointly form a hydrated film around the soil particles. The zeta potential, which is the potential difference between the NCSPs and the boundary of the diffusion layer, determines the thickness of this hydrated film. The thickness of the hydrated film directly affects the spacing between soil particles, thereby influencing the bonding between them. When the dispersant contains low-valence cations,

the cations in the Stern layer consume fewer negative charges from the NCSPs, resulting in a higher retention of negative charge within the NCSPs. Consequently, the zeta potential is higher, leading to a thicker hydrated film. A thicker hydrated film results in greater spacing between soil particles and a weaker bond among them. This makes it difficult for soil particles to aggregate and adhere, thus achieving the purpose of mud cake disintegration.

Mud cake samples that are immersed in solutions of sodium silicate, sodium hexametaphosphate, and oxalic acid experience ionic exchanges due to the strong hydration capabilities of monovalent Na^+ and H^+ ions. These ions replace the Ca^{2+} ions dissociated from the surfaces of clay particles and adhere to the surfaces of soil particles. This results in an increase in zeta potential, an augmented number of cations in the diffusion layer, enhanced hydration around clay particles, and reduced interparticle adhesion force, ultimately facilitating the disintegration of the mud cake samples. Conversely, if the dispersant contains high-valence cations, the cations in the Stern layer consume more negative charges from the NCSPs, leading to a reduced retention of negative charges within the NCSPs. Consequently, the zeta potential is lower, the hydrated film is thinner, and the disintegration of the mud cake is less pronounced.

2.3.2. Design of Disintegration Experiment

The float device in the traditional disintegration experiment is difficult to calibrate effectively, leading to low precision. In addition, due to the curved bucket body, it is difficult to accurately and read in real time in the traditional disintegration experiment instrument. To address these issues, an improved disintegration experimental instrument is proposed by connecting a high-precision electronic dynamometer to a computer to measure and record the mass changes in the mud cake samples after immersion over time, which can accurately record the dynamic process of mud cake disintegration.

The improved disintegration experiment instrument comprises a transparent square box ($25\text{ cm} \times 25\text{ cm} \times 25\text{ cm}$), a mesh plate with $1\text{ cm} \times 1\text{ cm}$ holes measuring $10\text{ cm} \times 10\text{ cm}$, and an electronic dynamometer with a 200 N range and $\pm 0.5\%$ accuracy. Additional components include fine rope, a bracket, and a computer (Figure 8).

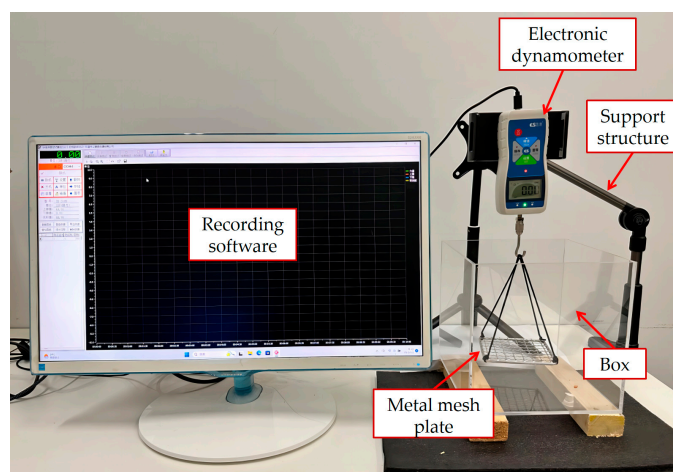


Figure 8. Improved disintegration experiment instrument.

After the instrument is installed, we connect the electronic dynamometer to the computer and set the electronic dynamometer recording software to record data every 0.1 s. Then, we pour the solution into the box. When the electronic dynamometer reading is stable, we reset the electronic dynamometer reading to zero.

Subsequently, the mud cake sample is slowly immersed into the solution and placed on the mesh plate to wait for its disintegration. The disintegrated matter falls through the holes of the mesh plate into the bottom of the square box, with the reading of the electronic dynamometer continuously decreasing throughout the disintegration process.

As the reading of the electronic dynamometer stabilizes, the recording is stopped, and the data are saved.

By using the electronic dynamometer, the mass changes in the mud cake sample can be measured relatively accurately. Subsequently, the disintegration amount (DA) of mud cake can be calculated using Equation (1), denoted as A_t . The disintegration amount at the completion of mud cake disintegration is referred to as the final disintegration amount (FDA).

$$A_t = \frac{F_0 - F_t}{F_0} \times 100\% \tag{1}$$

where A_t represents the amount of disintegration of the sample at time t ; F_0 and F_t are the electronic dynamometer values shown by the electronic dynamometer at the beginning of the test and time t , respectively; and the unit is N .

The final disintegration rate (FDR), denoted as V_T , is utilized to characterize the speed of the entire disintegration process. The calculation is defined by Equation (2).

$$V_T = \frac{A_T}{T} \tag{2}$$

where V_T represents the final disintegration rate of the sample at time T upon the completion of disintegration, and A_T is the final disintegration amount (FDA) at the completion of disintegration.

3. Results

3.1. Disintegration of Mud Cake Samples in Pure Water

Figure 9 illustrates the disintegration results for mud cake samples with thicknesses of 1 cm, 3 cm, and 5 cm in pure water. Initially, for the 3 cm thick sample (PW-T3), surface fine particles swiftly detached, as shown in Figure 10a. As the immersion time increased, water penetrated more deeply, causing fine soil particles on the surface to detach progressively. This led to crack expansions within the soil, resembling a “landslide” in the mud cake sample and resulting in the detachment of larger soil masses (Figure 10b). The end of disintegration was assessed by observing the mud cake’s condition and the electronic dynamometer’s readings. Disintegration concluded when particle detachment slowed and electronic dynamometer readings stabilized (Figure 10c). At this point, the corresponding value ($F_0 - F_t$) and the disintegration time (t) were recorded, and the DA, FDA and FDR were calculated by Equations (1) and (2), with the FDA being approximately 81%, the time 420 s, and the FDR $1.99 \times 10^{-3} \text{ s}^{-1}$.

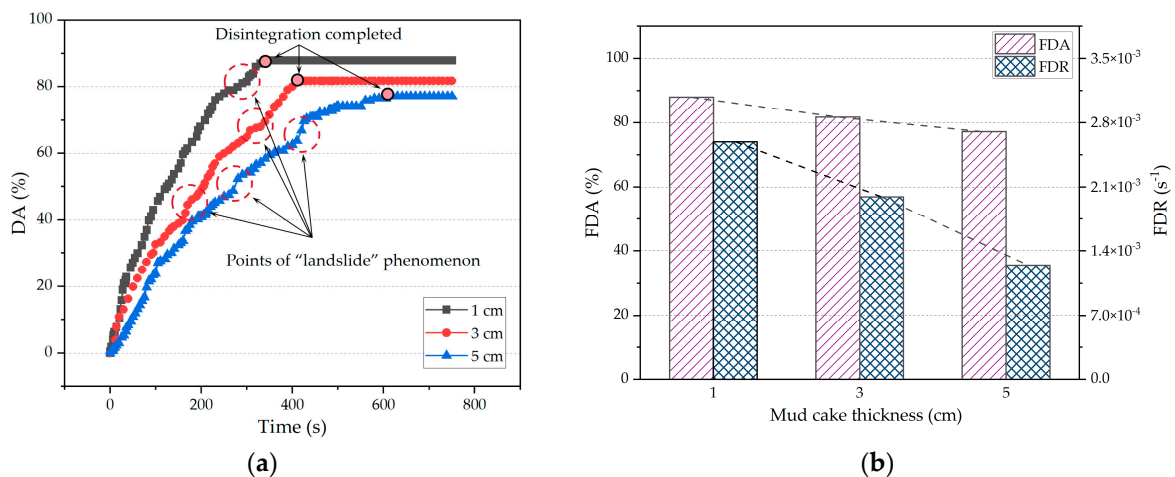


Figure 9. Disintegration of mud cake of different thickness in pure water. (a) Disintegration amount (DA)–time; (b) final disintegration amount (FDA)–final disintegration rate (FDR).

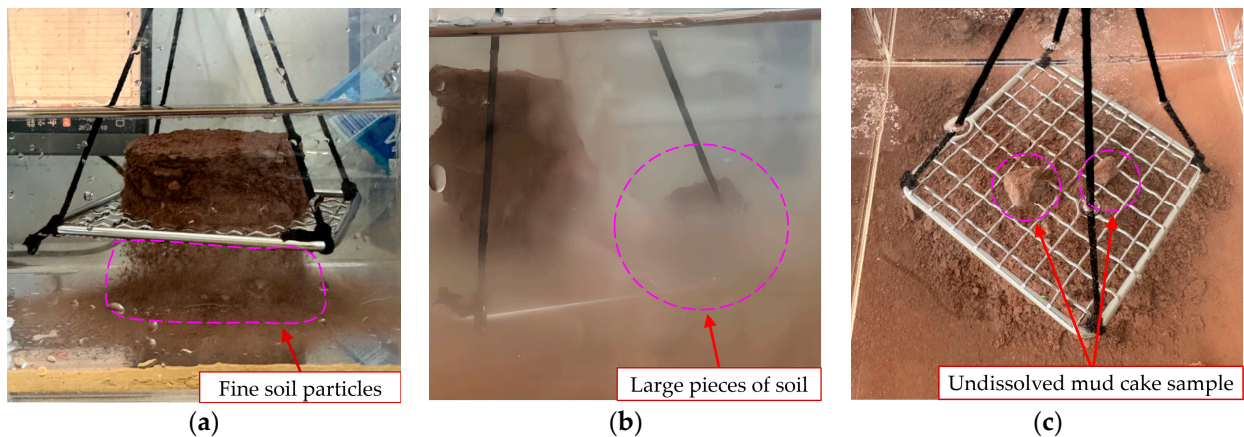


Figure 10. Disintegration process of specimen PW-T3. (a) Early stage of disintegration; (b) mid-stage of disintegration; (c) final stage of disintegration.

The 1 cm thick mud cake sample (PW-T1) exhibited disintegration processes and characteristics similar to PW-T3 but with a 30.2% increase in FDR, resulting in a faster overall process, a final disintegration time of 350 s, and an FDA of 88%. The disintegration characteristics of PW-T1 and PW-T3 were linear. The 5 cm thick mud cake sample (PW-T5) showed different disintegration characteristics from PW-T1 and PW-T3, with a longer disintegration time of 470 s and a larger remaining undissolved portion, culminating in an FDA of 77%.

The comparison presented in Figure 9b indicates that the PW-T5 sample took the longest time to disintegrate, approximately 34% longer than the 1 cm mud cake and about 12% longer than the 3 cm mud cake. Although the process was relatively smooth, it required 5 times more material than the 1 cm mud cake and 67% more than the 3 cm mud cake.

The disintegration times and characteristics of specimens PW-T1 and PW-T3 were similar. However, the PW-T1 specimen, with a thickness of 1 cm, had a smaller volume and exhibited a faster disintegration rate. This acceleration was especially pronounced in the presence of dispersants during subsequent tests, which could have complicated the accurate documentation of the mud cake's disintegration characteristics. Therefore, for subsequent experiments, a 3 cm thick mud cake sample was chosen.

In summary, as the thickness of the mud cake increases, the FDA of the mud cake gradually decreases, and the time for complete disintegration becomes longer. This may be due to the fact that as the thickness of the mud cake increases, the distance for internal water diffusion becomes longer, leading to a slower disintegration process.

3.2. Disintegration of Mud Cake Samples in Sodium Silicate Solution

As depicted in Figure 11, the FDA of the mud cake sample in 2%, 4%, 6%, and 8% sodium silicate solutions were lower than that in pure water, corresponding to 72%, 24%, 15%, and 87% of the disintegration observed in pure water, respectively. In the sodium silicate solution, the mud cake disintegrated slowly, initially producing foam and causing the solution to become cloudy over time, as illustrated in Figure 12. Interestingly, the disintegration percentage decreased initially with increasing concentrations of the solution but then increased.

The disintegration times for specimens SS-T3-P2, SS-T3-P4, SS-T3-P6, and SS-T3-P8 were recorded at 480 s, 360 s, 260 s, and 250 s, respectively, with corresponding FDR values of $1.23 \times 10^{-3} \text{ s}^{-1}$, $5.331 \times 10^{-4} \text{ s}^{-1}$, $4.76 \times 10^{-4} \text{ s}^{-1}$, and $2.83 \times 10^{-3} \text{ s}^{-1}$. Remarkably, only the 8% sodium silicate solution exhibited an FDR marginally higher than that observed in pure water ($1.99 \times 10^{-3} \text{ s}^{-1}$), although the FDA remained lower than that achieved with pure water.

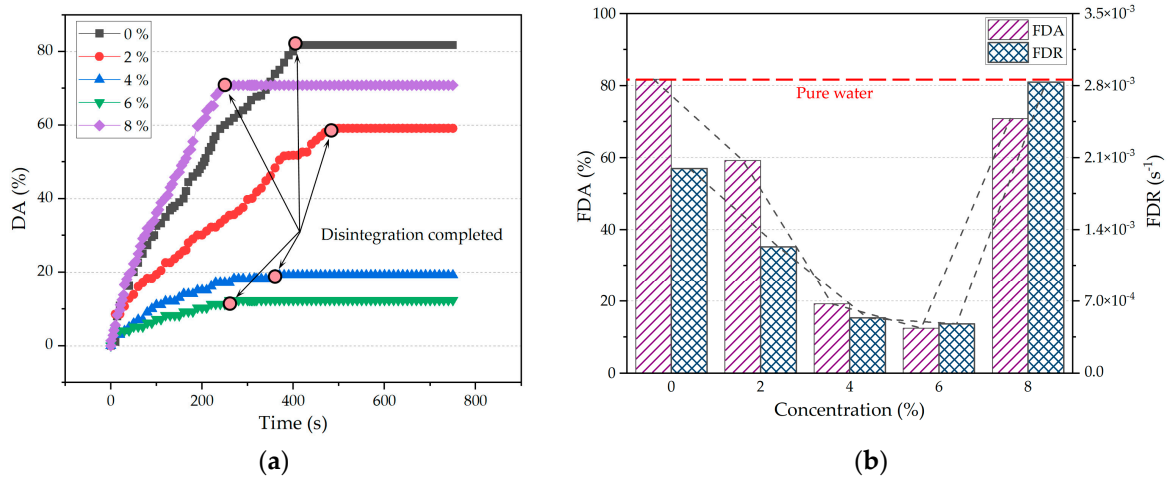


Figure 11. The disintegration of mud cake in sodium silicate solution. (a) Disintegration amount (DA)–time; (b) final disintegration amount (FDA)–final disintegration rate (FDR).

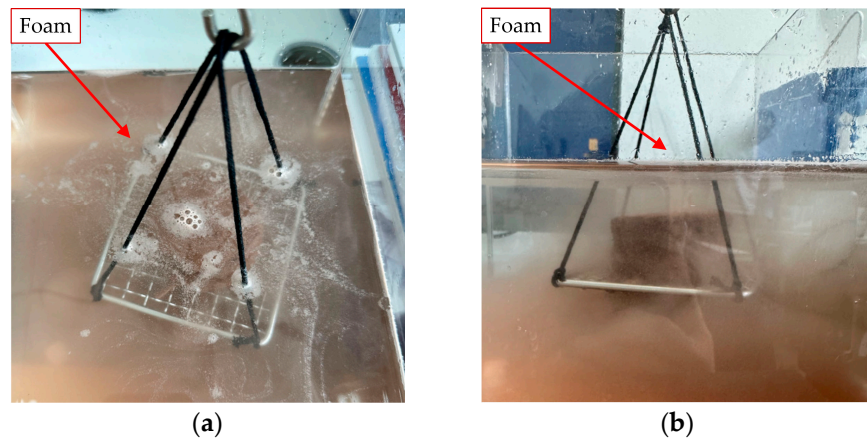
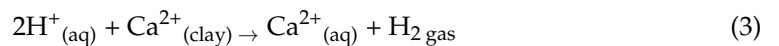


Figure 12. Disintegration process of specimen SS-T3-P8. (a) Early stage of disintegration; (b) final stage of disintegration.

The consistently lower disintegration effect observed in sodium silicate solution compared to pure water could be attributed to the abundant iron ions present in the red-bed geology. These ions readily formed calcium–iron silicate precipitates with the sodium silicate. These precipitates formed robust adhesions to the soil particle surfaces and clogged interparticle pores, significantly inhibiting the disintegration of the mud cake.

3.3. Disintegration of Mud Cake Samples in Oxalic Acid Solution

Oxalic acid (H₂C₂O₄) releases H⁺ ions when the mud cake samples are immersed in an oxalic acid solution. These ions react with the calcium ions in the clay to form soluble calcium salts and release gas, as depicted in chemical Equation (3).



This reaction initiates foam formation on the surface of the solution, leading to the gradual dissolution of the mud cake and the formation of a cloudy suspension.

Samples OA-T3-P10 and OA-T3-P15 quickly reached a state of rapid disintegration (Figure 13), achieving nearly 50% disintegration within the first 10 s, displaying similar disintegration characteristics. Although the rate of disintegration subsequently decreased, it remained significantly high. Around 230 s, as the solution further penetrated, there was a marked increase in the disintegration rate, characterized by intensified foam production

and increased cloudiness (Figure 14). Eventually, both samples completed the disintegration process, with completion times of 240 s and 280 s, respectively. The FDR were $4.17 \times 10^{-3} \text{ s}^{-1}$ and $3.57 \times 10^{-3} \text{ s}^{-1}$, respectively, approximately 109% and 79% higher than the FDR observed in pure water.

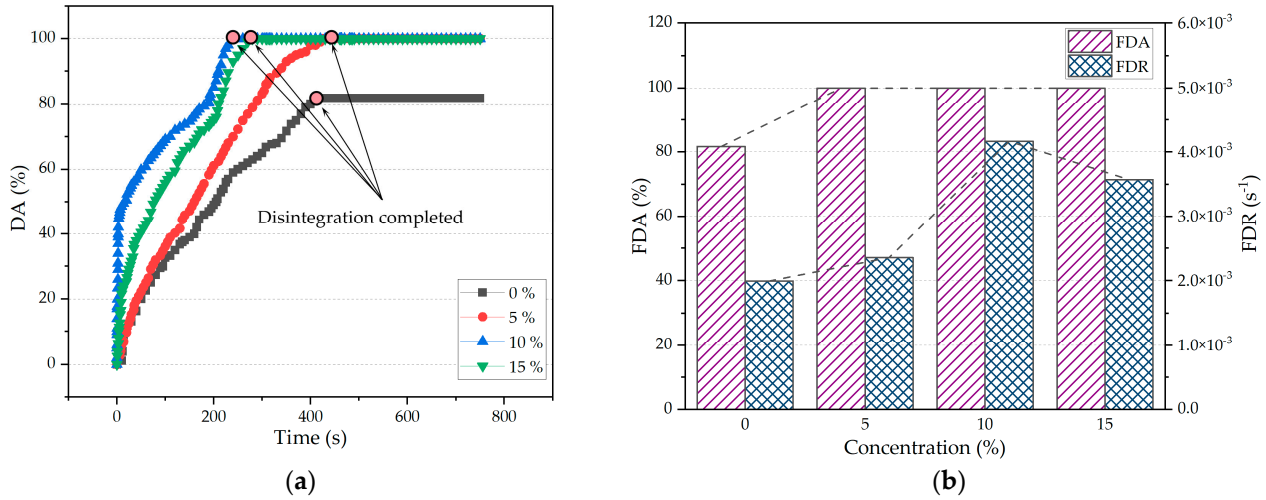


Figure 13. The disintegration of mud cake in oxalic acid solution. (a) Disintegration amount (DA)–time; (b) final disintegration amount (FDA)–final disintegration rate (FDR).

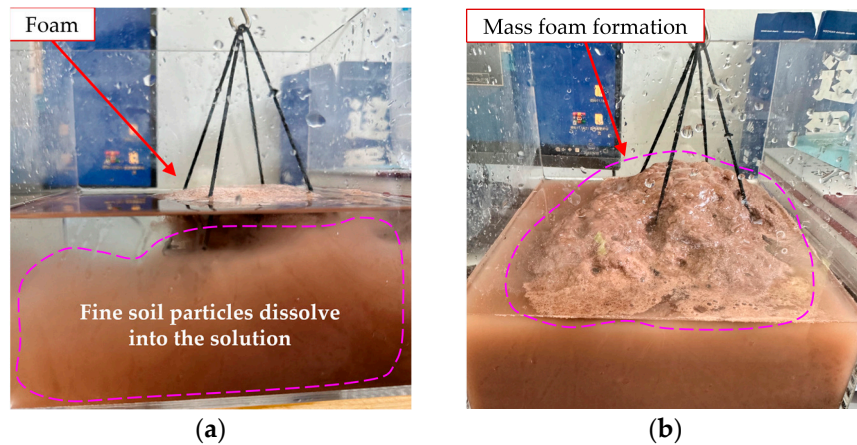


Figure 14. Disintegration process of specimen OA-T3-P10. (a) Early stage of disintegration; (b) final stage of disintegration.

The mud cake sample (OA-T3-P5) also completely disintegrated in a 5% oxalic acid solution, but the disintegration time was 425 s, with an FDR of $2.35 \times 10^{-3} \text{ s}^{-1}$. Compared to the disintegration process in the 10% oxalic acid solution, the rate was approximately 44% slower. This indicates that a 10% concentration of oxalic acid solution is optimal for achieving efficient disintegration.

3.4. Disintegration of Mud Cake Samples in Sodium Hexametaphosphate Solution

Figure 15 demonstrates the disintegration process of mud cake samples in sodium hexametaphosphate solution. The disintegration characteristics across sodium hexametaphosphate solution concentrations of 2% (SH-T3-P2), 4% (SH-T3-P4), 6% (SH-T3-P6), and 8% (SH-T3-P8) appear consistent, displaying a pattern similar to the dual-line graph of AB and BC (Figure 15a).

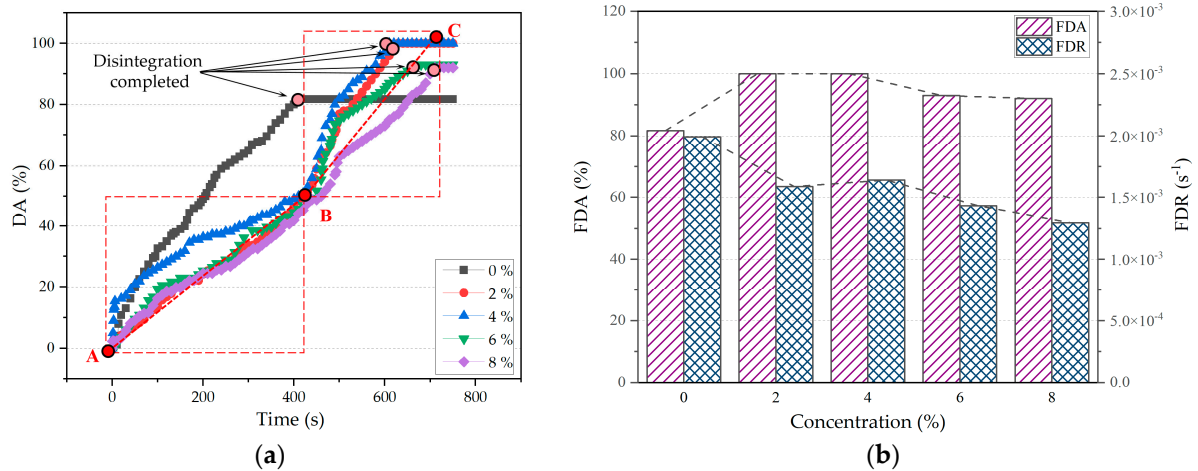


Figure 15. The disintegration of mud cake in sodium hexametaphosphate solution. (a) Disintegration amount (DA)–time; (b) final disintegration amount (FDA)–final disintegration rate (FDR).

In the *AB* segment, water permeated from the surface inward, causing dry soil particles on the sample's surface to detach and disintegrate upon contact with water (Figure 16a). In the *BC* section, at around 440 s, the interaction between the solution and mud cake particles led to large soil mass slippages, accelerating the disintegration rate, generating a lot of foam, and increasing solution turbidity (Figure 16b). Finally, the disintegration concluded within 640 s (Figure 16c). The speed of segment *BC* was significantly faster than that of segment *AB*.

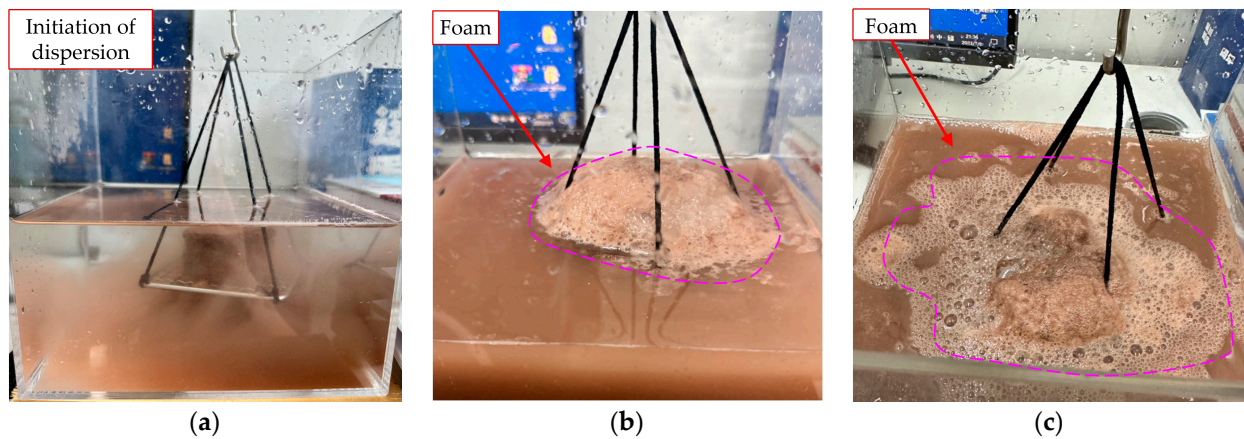


Figure 16. Disintegration process of specimen SH-T3-P2. (a) Early stage of disintegration; (b) mid-stage of disintegration; (c) final stage of disintegration.

Complete disintegration was observed for SH-T3-P2 and SH-T3-P4 samples. However, the FDA for SH-T3-P6 and SH-T3-P8 were 93% and 92%, indicating partial disintegration. The final disintegration times for SH-T3-P2, SH-T3-P4, SH-T3-P6, and SH-T3-P8 were 630 s, 610 s, 650 s, and 710 s, respectively, with FDR of $1.59 \times 10^{-3} \text{ s}^{-1}$, $1.64 \times 10^{-3} \text{ s}^{-1}$, $1.43 \times 10^{-3} \text{ s}^{-1}$, and $1.29 \times 10^{-3} \text{ s}^{-1}$, all below the rate in pure water.

Given the effective disintegration observed with 2% and 4% sodium hexametaphosphate solutions and the minimal difference between them, a 2% solution is deemed the optimal concentration.

3.5. Recommended Dispersant Concentration

Experiments were conducted on sodium silicate (SS) solution, oxalic acid (OA) solution, and sodium hexametaphosphate (SH) solution, with their optimal concentrations

determined to be 8%, 10%, and 2%, respectively. Based on these optimal concentrations, a comparative analysis of their disintegration effects was performed, as shown in Figure 17.

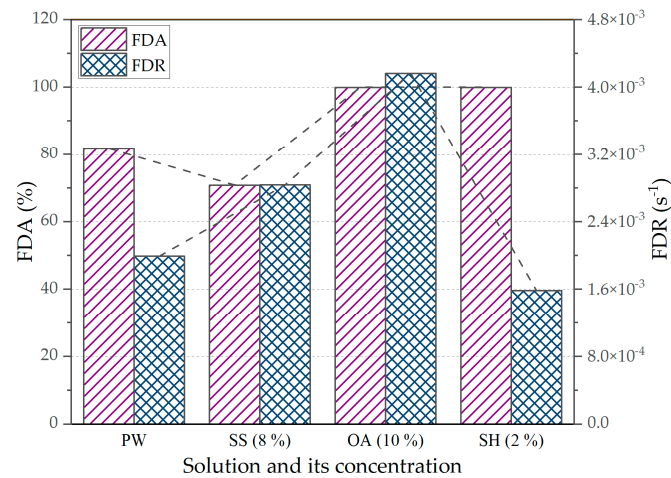


Figure 17. Final disintegration amount (FDA) and final disintegration rate (FDR) of mud cake sample under the optimal concentration of each dispersant.

The mud cake in the 10% oxalic acid solution and 2% sodium hexametaphosphate solution both disintegrated completely, but the 10% oxalic acid solution disintegrated faster, took less time to complete the disintegration, and the overall effect was better. Therefore, in actual engineering projects, it is recommended to use the 10% oxalic acid solution as dispersant.

3.6. Engineering Application

As the shield machine of the west line tunneled near Ring 173, the soil layer there was relatively complex, primarily consisting of limonite-calcified silty mudstone, which resulted in high torque, slow speed, and significant fluctuations in tunneling parameters. A comprehensive analysis implied that mud caking had occurred on the cutterhead. Therefore, at Ring 180, after ensuring the stability of the excavation face, the shield machine stopped tunneling to perform cutter replacement and mud cake removal. Figure 18 shows the cutter replacement operation, and Figure 19 displays the mud cake adhered to the cutter.

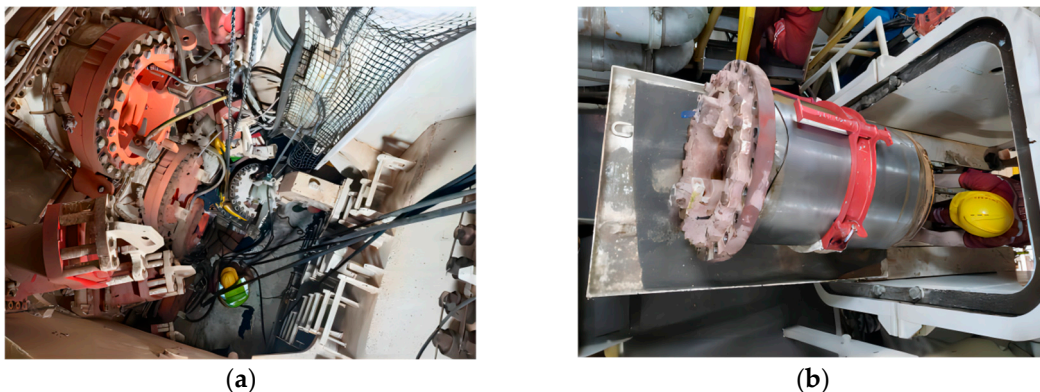


Figure 18. Operation of opening the chamber and replacing the cutter. (a) Excavation chamber operation; (b) replacing the cutter.



Figure 19. Mud cake adhering to the cutter. (a) MA6 rolling cutter, (b) MA2 rolling cutter.

The 10% oxalic acid solution was injected into the excavation chamber through the central jetting system and allowed to soak for 24 h. Through intermittent forward and reverse rotations of the cutterhead, the mud cake adhered to the cutterhead was dispersed and eliminated. After 24 h, the shield machine resumed normal tunneling, and the subsequent tunneling parameters were monitored. Figure 20 presents the tunneling speed and torque between Rings 165 and 200.

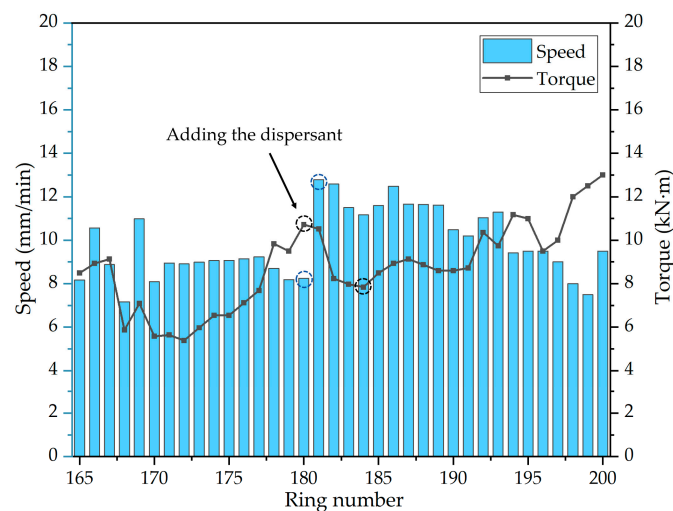


Figure 20. Changes in excavation parameters before and after injection.

After the dispersant was injected, the torque of the shield machine decreased from 10.72 kNm at Ring 180 to 7.98 kNm at Ring 184, and the tunneling speed increased from 8.25 mm/min at Ring 180 to 12.79 mm/min at Ring 181. The injection of the dispersant solution significantly improved the tunneling performance of the shield machine. This indicates that the 10% oxalic acid solution has an excellent dispersing effect on the mud cake in red-bed geology, enhancing the tunneling efficiency of the shield machine. At the same time, it also verifies the reliability of the results from laboratory experiments.

4. Discussion

The study revealed that mud cake samples completely disintegrated in the 4% sodium hexametaphosphate solution. However, as the concentration increased, the final disintegration amount decreased to 93% in the 6% solution and further dropped to 92% in the 8% solution. Similarly, when using the 15% oxalic acid solution, the time required for complete disintegration of the mud cake extended to 280 s, approximately 17% longer than the 240 s observed at the 10% concentration. These findings suggest that beyond a certain threshold, higher concentrations of dispersant solutions begin to inhibit the disintegration of mud cake.

As the concentration of the dispersant solution exceeds its threshold, an increase in the concentration of cations in the solution is observed, enhancing the likelihood of cations entering the Stern layer. Consequently, a higher number of cations in the Stern layer results in excessive neutralization of the negative charges of the NCSPs. This leads to a reduction in the zeta potential, the thinning of the diffusion layer and the hydrated film, and a transition of the dispersion system from a dispersed to a flocculated state, thereby diminishing the disintegration effect. This process is illustrated in Figure 21.

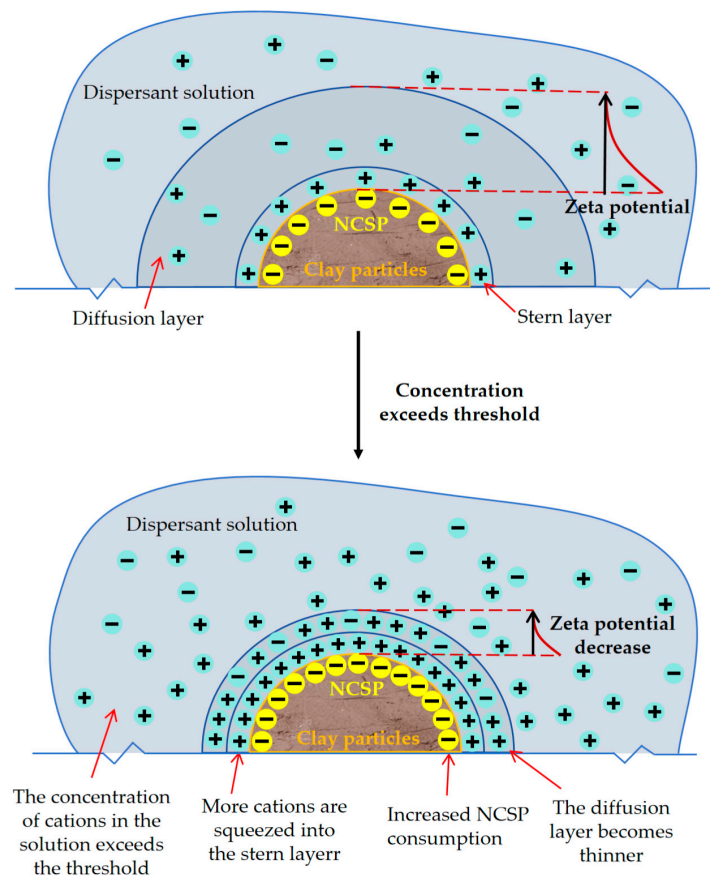


Figure 21. Mechanism diagram of concentration exceeding threshold.

5. Conclusions

An improved mud cake disintegration experimental instrument was developed, and the disintegration characteristics of mud cake samples in pure water were assessed to establish the use of 3 cm thick mud cakes for dispersants disintegration experiments. The dispersant disintegration experiments were conducted and the conclusions are as follows:

The experiments demonstrated that a 10% oxalic acid solution is most effective in disintegrating mud cakes from red-bed geology. Oxalic acid was applied in practical engineering with good effect.

The final disintegration amount of mud cake samples in sodium silicate solution was consistently lower than in pure water. In addition, the disintegration effect of sodium hexametaphosphate solution on red-bed geological mud cake was positive, but its effect was not as good as oxalic acid, and its optimal disintegration concentration was 2%. Therefore, neither of these dispersants is recommended.

In the disintegration of red-bed geological mud cake, the concentration of dispersant has threshold effect. Once the concentration of the dispersant solution exceeds its threshold, the effect of decomposition will be reduced. The threshold concentrations of sodium hexametaphosphate and oxalic acid solutions were 4% and 10%, respectively.

Author Contributions: Writing—original draft, J.Y.; project administration, writing—review and supervision, X.X.; investigation, C.G.; methodology, conceptualization, data analysis, writing—review, K.Z. All authors have read and agreed to the published version of the manuscript.

Funding: This research received no external funding.

Institutional Review Board Statement: Not applicable.

Informed Consent Statement: Not applicable.

Data Availability Statement: All data that support the findings of this study are available from the corresponding author upon reasonable request.

Conflicts of Interest: The authors declare no conflicts of interest.

References

1. Heuser, M.; Spagnoli, G.; Leroy, P.; Klitzsch, N.; Stanjek, H. Electro-osmotic flow in clays and its potential for reducing clogging in mechanical tunnel driving. *Bull. Eng. Geol. Environ.* **2012**, *71*, 721–733. [\[CrossRef\]](#)
2. Khabbazi, A.; Ghafoori, M.; Tarigh Azali, S.; Cheshomi, A. Experimental and laboratory assessment of clogging potential based on adhesion. *Bull. Eng. Geol. Environ.* **2019**, *78*, 605–616. [\[CrossRef\]](#)
3. Basmenj, A.K.; Ghafoori, M.; Cheshomi, A.; Azandariani, Y.K. Adhesion of clay to metal surface; Normal and tangential measurement. *Geomech. Eng.* **2016**, *10*, 125–135. [\[CrossRef\]](#)
4. Wang, R.; Xu, H.; Liu, Y.; Jiang, P.; Zhou, A. Reusing Fine Silty Sand Excavated from Slurry Shield Tunnels as a Sustainable Raw Material for Synchronous Grouting. *Coatings* **2023**, *13*, 398. [\[CrossRef\]](#)
5. Djeran-Maigre, I.; Dubujet, P.; Vogel, T.M. Variation over time of excavated soil properties treated with surfactants. *Environ. Earth Sci.* **2018**, *77*, 67. [\[CrossRef\]](#)
6. Zhang, Z.M.; Lin, C.G.; Wu, S.M. Slurry shield tunnelling in clayey soils: Typical problems and countermeasures. *Adv. Mater. Res.* **2011**, *243*, 2944–2947. [\[CrossRef\]](#)
7. Umar, I.H.; Lin, H.; Ibrahim, A.S. Laboratory Testing and Analysis of Clay Soil Stabilization Using Waste Marble Powder. *Appl. Sci.* **2023**, *13*, 9274. [\[CrossRef\]](#)
8. Sousa, R.L.; Einstein, H.H. Lessons from accidents during tunnel construction. *Tunn. Undergr. Space Technol.* **2021**, *113*, 103916. [\[CrossRef\]](#)
9. Koopialipoor, M.; Fahimifar, A.; Ghaleini, E.N.; Momenzadeh, M.; Armaghani, D.J. Development of a new hybrid ANN for solving a geotechnical problem related to tunnel boring machine performance. *Eng. Comput.* **2020**, *36*, 345–357. [\[CrossRef\]](#)
10. Alija, S.; Torrijo, F.; Quinta-Ferreira, M. Geological engineering problems associated with tunnel construction in karst rock masses: The case of Gavarres tunnel (Spain). *Eng. Geol.* **2013**, *157*, 103–111. [\[CrossRef\]](#)
11. Farrokh, E.; Kim, D.Y. A discussion on hard rock TBM cutter wear and cutterhead intervention interval length evaluation. *Tunn. Undergr. Space Technol.* **2018**, *81*, 336–357. [\[CrossRef\]](#)
12. Xu, Y.; Liu, Q.; Zhi, W.; Shao, G.; Liu, P. Long-Distance Freezing Design and Construction Based on Monitoring Analysis of Subway Connection Aisle. *Coatings* **2024**, *14*, 355. [\[CrossRef\]](#)
13. Mei, Y.; Zhou, D.; Gong, H.; Ke, X.; Xu, W.; Shi, W. Study on comprehensive technology of preventing mud cake of large diameter slurry shield in composite stratum. *Buildings* **2022**, *12*, 1555. [\[CrossRef\]](#)
14. Tsubaki, J.; Mori, T.; Tseveen, U.; Bayanjargal, O. Development of a novel slurry condensation method by applying dispersant instead of flocculant. *Adv. Powder Technol.* **2009**, *20*, 106–110. [\[CrossRef\]](#)
15. Zhao, S.; Li, S.; Wan, Z.; Wang, M. Dispersant for reducing mud cakes of slurry shield tunnel boring machine in sticky ground. *Adv. Mater. Sci. Eng.* **2021**, *2021*, 5524489. [\[CrossRef\]](#)
16. Langmaack, L. Advanced technology of soil conditioning in EPB shield tunnelling. *Proc. N. Am. Tunneling* **2000**, *2000*, 525–542.
17. Langmaack, L. Europe & Asia: Application of new TBM conditioning additives. In Proceedings of the BAUMA 2001, Munich, Germany, 2–8 April 2001; Volume 3, pp. 88–92.
18. Martinotto, A.; Langmaack, L. Toulouse Metro Lot 2: Soil conditioning in difficult ground conditions. In Proceedings of the ITA-AITES World Tunnel Congress, Prague, Czech Republic, 5–10 June 2007; pp. 1211–1216.
19. Wang, S.; Liu, P.; Hu, Q.; Zhong, J. Effect of dispersant on the tangential adhesion strength between clay and metal for EPB shield tunnelling. *Tunn. Undergr. Space Technol.* **2020**, *95*, 103144. [\[CrossRef\]](#)
20. Zumsteg, R.; Puzrin, A.M.; Anagnostou, G. Effects of slurry on stickiness of excavated clays and clogging of equipment in fluid supported excavations. *Tunn. Undergr. Space Technol.* **2016**, *58*, 197–208. [\[CrossRef\]](#)
21. de Oliveira, D.G.; Thewes, M.; Diederichs, M.S. Clogging and flow assessment of cohesive soils for EPB tunnelling: Proposed laboratory tests for soil characterisation. *Tunn. Undergr. Space Technol.* **2019**, *94*, 103110. [\[CrossRef\]](#)
22. Thewes, M.; Budach, C. Parameters for soil conditioning with foam in coarse-grained soils with epb-shields. In Proceedings of the World Tunnel Congress, Vancouver, BC, Canada, 14–20 May 2010.
23. Thewes, M.; Budach, C.; Bezuijen, A. Foam conditioning in EPB tunnelling. In *Geotechnical Aspects of Underground Construction in Soft Ground*; CRC Press: Boca Raton, FL, USA, 2012; Volume 127.

24. Zumsteg, R.; Plötze, M.; Puzrin, A.M. Effect of soil conditioners on the pressure and rate-dependent shear strength of different clays. *J. Geotech. Geoenvironmental Eng.* **2012**, *138*, 1138–1146. [[CrossRef](#)]
25. Feinendegen, M.; Ziegler, M.; Spagnoli, G.; Fernández-Steeger, T. Evaluation of the clogging potential in mechanical tunnel driving with EPB-shields. In Proceedings of the 15th European Conference on Soil Mechanics and Geotechnical Engineering, Athens, Greece, 12–15 September; 2011; pp. 1633–1638.
26. Feinendegen, M.; Ziegler, M.; Spagnoli, G.; Fernández-Steeger, T.; Stanjek, H. A new laboratory test to evaluate the problem of clogging in mechanical tunnel driving with EPB-shields. In *Rock Mechanics in Civil and Environmental Engineering*; CRC Press: Boca Raton, FL, USA, 2010; pp. 429–432.
27. Spagnoli, G.; Feinendegen, M.; Rubinos, D. Modification of clay adhesion to improve tunnelling excavation. *Proc. Inst. Civ. Eng. Ground Improv.* **2013**, *166*, 21–31. [[CrossRef](#)]
28. Ren, G.; Zhang, J.; Feng, T.; Liang, Y.; Yin, Y. Mechanism and Influence of Dispersants on the Action of Polymer Flocculants Used in Slurry Separation. *Polymers* **2023**, *15*, 4073. [[CrossRef](#)] [[PubMed](#)]
29. Sun, Y.; Zhao, D. Research and Experimental Application of New Slurry Proportioning for Slag Improvement of EPB Shield Crossing Sand and Gravel Layer. *Coatings* **2022**, *12*, 1961. [[CrossRef](#)]
30. Grassi, R.; Daghetti, A.; Trasatti, S. Application of the Gouy-Chapman-Stern-Grahame model of the electrical double layer to the determination of single ion activities of KF aqueous solutions. *J. Electroanal. Chem. Interfacial Electrochem.* **1987**, *226*, 341–349. [[CrossRef](#)]
31. Rehl, B.; Ma, E.; Parshotam, S.; DeWalt-Kerian, E.L.; Liu, T.; Geiger, F.M.; Gibbs, J.M. Water structure in the electrical double layer and the contributions to the total interfacial potential at different surface charge densities. *J. Am. Chem. Soc.* **2022**, *144*, 16338–16349. [[CrossRef](#)]
32. Li, Y.; Weng, L.; Wu, L.; Gong, H.; Zhang, Y.; Zhang, R.; Shen, J.; Yin, Y.; Alves, M.E.; Zhou, D. Combining multisurface model and Gouy–Chapman–Stern model to predict cadmium uptake by cabbage (*Brassica Chinensis* L.) in soils. *J. Hazard. Mater.* **2021**, *416*, 126260. [[CrossRef](#)]
33. Chan, D.Y.; Healy, T.W.; Supasiti, T.; Usui, S. Electrical double layer interactions between dissimilar oxide surfaces with charge regulation and Stern–Grahame layers. *J. Colloid Interface Sci.* **2006**, *296*, 150–158. [[CrossRef](#)]

Disclaimer/Publisher’s Note: The statements, opinions and data contained in all publications are solely those of the individual author(s) and contributor(s) and not of MDPI and/or the editor(s). MDPI and/or the editor(s) disclaim responsibility for any injury to people or property resulting from any ideas, methods, instructions or products referred to in the content.